Biol. Cybern. 80, 291–297 (1999)

Biological Cybernetics

Coefficient of variation of interspike intervals greater than 0.5. How and when?

Jianfeng Feng, David Brown

Computational Neuroscience Laboratory, The Babraham Institute, Cambridge CB2 4AT, UK

Received: 25 June 1998 / Accepted in revised form: 16 December 1998

Abstract. Using Stein's model with and without reversal potentials, we investigated the mechanism of production of spike trains with a CV (ISI) (standard deviation/mean interspike interval) greater than 0.5, as observed in the visual cortex. When the attractor of the deterministic part of the dynamics is below the firing threshold, spike generation results primarily from random fluctuations. Using computer simulation for a range of membrane decay times and with other model parameters set to values appropriate for the visual cortex, we demonstrate that CV (ISI) is then usually greater than 0.5; if the attractor is above the threshold, spike generation is mainly due to deterministic forces, and CV (ISI) is then usually lower than 0.5. The critical value of the inhibitory postsynaptic potential (IPSP) rate at which CV (ISI) becomes greater than 0.5 is determined, resulting in specifications of how neurones might adjust their synaptic inputs to elicit irregular spike trains.

1 Introduction

In vivo cell recordings show that most neurones fire irregularly. For example, the coefficient of variation (CV), of interspike intervals (ISIs), of neurones in the visual cortex of the monkey is greater than 0.5 [28]. A comparison between in vitro and in vivo experiments strongly supports the assertion that the irregularity results from input from other neurones, both inhibitory and excitatory [14]. How does the variability of the elicited spike train relate to the characteristics of the synaptic input? This is a fundamental question and one of the central themes in computational neuroscience [17, 30]. A better understanding of the origins of irregularity in spike trains will help us to elaborate general principles of neuronal circuitry [20, 21, 25–27] and to test whether rate or timing coding is the fundamental mode of neural communication [12, 15, 27].

Correspondence to: J. Feng (e-mail: jf218@cam.ac.uk)

In this paper, using the leaky integrate-and-fire model (Stein's model), we explore how values of CV (ISI) (abbreviated to CV in the remainder of the paper) greater than 0.5 occur for physiologically plausible parameter regions. The firing mechanisms in these model neurones can operate in two ways. The first occurs when the passage of membrane potential to the firing threshold is essentially driven by *deterministic* forces (as defined below in Sect. 2.4), possibly supplemented or modified by random fluctuations; that is to say, without these fluctuations the neurone would fire regularly. In this case CV is usually less than 0.5. The other case occurs when the threshold is crossed primarily as a result of random fluctuations; in this case, without the fluctuations firing would not occur at all, and CV is normally greater than 0.5. This provides an answer to the question: how does CV greater than 0.5 occur? Using this theory, we also estimate how large an inhibitory postsynaptic potential (IPSP) rate (or alternatively what number of active inhibitory synapses) is needed for CV to reach 0.5. This answers the question: when does a CV greater than 0.5 occur? We provide evidence for these relationships for a range of parameter values using computer simulations of Stein's model.

To confirm our results using a slightly more realistic model, we consider a model with reversal potentials. Numerical simulations provide the same results as for the leaky integrator without reversal potentials. The number of inhibitory input synapses or the IPSP rate at which CV becomes greater than 0.5 closely matches the number at which random fluctuations are essential for threshold crossings to occur.

In recent years there has been much research on the output variability of single neurone models, see for example [8] and references therein. In particular (see also [23]), Troyer and Miller [32] have pointed out that if postspike voltage is reset to a value higher than the resting potential, the integrate-and-fire model is capable of producing efferent spike trains with a CV greater than 0.5. In the present paper and [8] where the behaviour of the perfect integrate-and-fire model was analysed, we show that there is a wide range of parameters within

which the integrate-and-fire model fires irregularly, with a CV greater than 0.5. We focus on Stein's model with or without reversal potentials, but without the device used by Troyer and Miller. A major purpose of the present paper is to clarify the underlying mechanisms of generation of irregular spike trains for the integrate-and-fire model. Our work thus differs from some earlier studies [32] both in the model used and the purpose of the investigation. Furthermore, to the best of our knowledge, no one has systematically carried out an analysis (confirmed by numerical simulations) of CV by linking it to the position of the equilibrium of the deterministic part of the single neurone dynamics, as we do here.

2 Models

2.1 Stein's model

The basic idea of Stein's model [7, 13, 34] is that neurones are integrate-and-fire devices charged with incoming excitatory postsynaptic potentials (EPSPs) and IPSPs. The inter-arrival times of single EPSPs and IPSPs are exponentially distributed with rate $N_E\lambda_E$ and $N_I\lambda_I$, respectively, where $N_E(N_I)$ is the number of afferent, excitatory (inhibitory) synapses and $\lambda_E(\lambda_I)$ is the rate of EPSPs (IPSPs) propagating along each synapse. The membrane potential V_t at time t is governed by

$$dV_t = -\frac{1}{\gamma}(V_t - V_{\text{rest}})dt + a \cdot dN_t^E - b \cdot dN_t^I \tag{1}$$

with $V_0 = V_{\text{rest}}$, where $a > 0$ and $b > 0$ are the magnitude of single EPSPs and IPSPs, V_{rest} is the resting potential, $1/\gamma$ the decay rate and N_t^E, N_t^I are Poisson processes with rate $N_E\lambda_E$ and $N_I\lambda_I$. Once the membrane potential crosses the threshold potential, V_{th}, a spike is elicited, and V_t is reset to V_{rest}. We take $V_{\text{rest}} = -50$ mV, V_{th} is 20 mV above the resting potential and $a = b = 0.5$ mV [30] for Stein's model.

2.2 Lower bounds on membrane potential

There is, however, a substantial problem for the model defined by (1). We know that the voltage of single neurones is bounded from below, about 10 mV below the resting potential, but V_t visits any negative value with a positive probability. There are several ways to prevent this from happening. One is simply to suppose the membrane potential is $V_t^+ = \max(V_t, V_{\text{rest}})$. The advantage of this modification is that all analytical results in the literature on the first exit time of V_t are valid for V_t^+ [13, 34]. Another way is to impose a lower boundary condition for V_t and thus obtain a new process v_t [30] which is defined in the following way.

$$\begin{cases} dv_t^{(n+1)} = -\frac{1}{\gamma}(v_t^{(n+1)} - V_{\text{rest}})dt + a \cdot dN_t^E - b \cdot dN_t^I \\ v_{\tau_{n+1}}^{(n+1)} = V_{\text{rest}} \end{cases} \tag{2}$$

Let $\tau_1 = 0$, $n \geq 0$, and define a sequence of stopping times by

$$\tau_{n+1} = \inf\{t : v_t^{(n)} < V_{\text{rest}}, t \geq \tau_n\}$$

v_t is then defined as $\sum_n v_t^{(n)} I_{\{\tau_n < t < \tau_{n+1}\}}$, where I is the indicator function. According to the definition above, it is easily seen that $v_t \geq V_{\text{rest}}$. Obviously, v_t and V_t or V_t^+ are different. Suppose that at time t_0, $V_{t_0} = V_{\text{rest}}$, and $V_t < V_{\text{rest}}$ for $t_0 < t < t_1$. V_t evolves according to (1) and therefore below the resting potential; for $t_0 < t < t_1$, V_t^+ remains at its resting potential, and any incoming EPSPs have no effect. Furthermore, the first passage times of V_t and V_t^+ are identical. v_t, however, responds to any incoming EPSPs, and therefore v_t is different from V_t, and their first passage times might be different. V_t^+ might spend a very long time at the resting potential and not respond to any incoming signals at all. The definition of v_t overcomes this drawback. Interestingly from numerical results (see Fig. 1), we conclude that if we concentrate on CV, which is the purpose of this paper, the behaviour of these two models is very close, and hence all theoretical results about CV of V_t are good approximations to those of v_t. In the remainder of this paper, we therefore confine ourselves to V_t.

The other, more biologically realistic modification is to include reversal potentials in Stein's model [23, 34]

$$dZ_t = -\frac{Z_t - V_{\text{rest}}}{\gamma}dt + \bar{a}(V_E - Z_t)dN_t^E + \bar{b}(V_I - Z_t)dN_t^I \tag{3}$$

Z_t is now a birth-and-death process with boundaries V_E and V_I where $V_I < V_{\text{rest}} < V_{\text{th}} < V_E$. Once Z_t is below V_{rest}, the decay term $Z_t - V_{\text{rest}}$ will increase membrane potential Z_t; whereas when Z_t is above V_{rest}, the decay term will reduce it.

2.3 Deterministic and stochastic components

Usually a discrete process like Stein's model (a birth-and-death process [6]) is hard to deal with theoretically, and so various approximations have been sought. The diffusion process [9] serves such a purpose [24, 34]:

$$dw_t = -\frac{1}{\gamma}(w_t - V_{\text{rest}})dt + \mu\,dt + \sigma\,dB_t \tag{4}$$

with $w_0 = V_{\text{rest}}$, where B_t is standard Brownian motion and

$$\mu = aN_E\lambda_E - bN_I\lambda_I \qquad \sigma^2 = a^2N_E\lambda_E + b^2N_I\lambda_I \tag{5}$$

More generally, a stochastic dynamical system can be expressed as

$$dX_t = b(X_t)dt + \sigma(X_t)dM_t \tag{6}$$

where $b, \sigma \in C^\infty(IR)$ and M_t is an L^2-martingale. We define the following dynamics

$$dEX_t = Eb(X_t)dt \tag{7}$$

as the deterministic part of X_t where E is expectation [3]. Note that V_t, w_t and Z_t are all of form (6). For example,

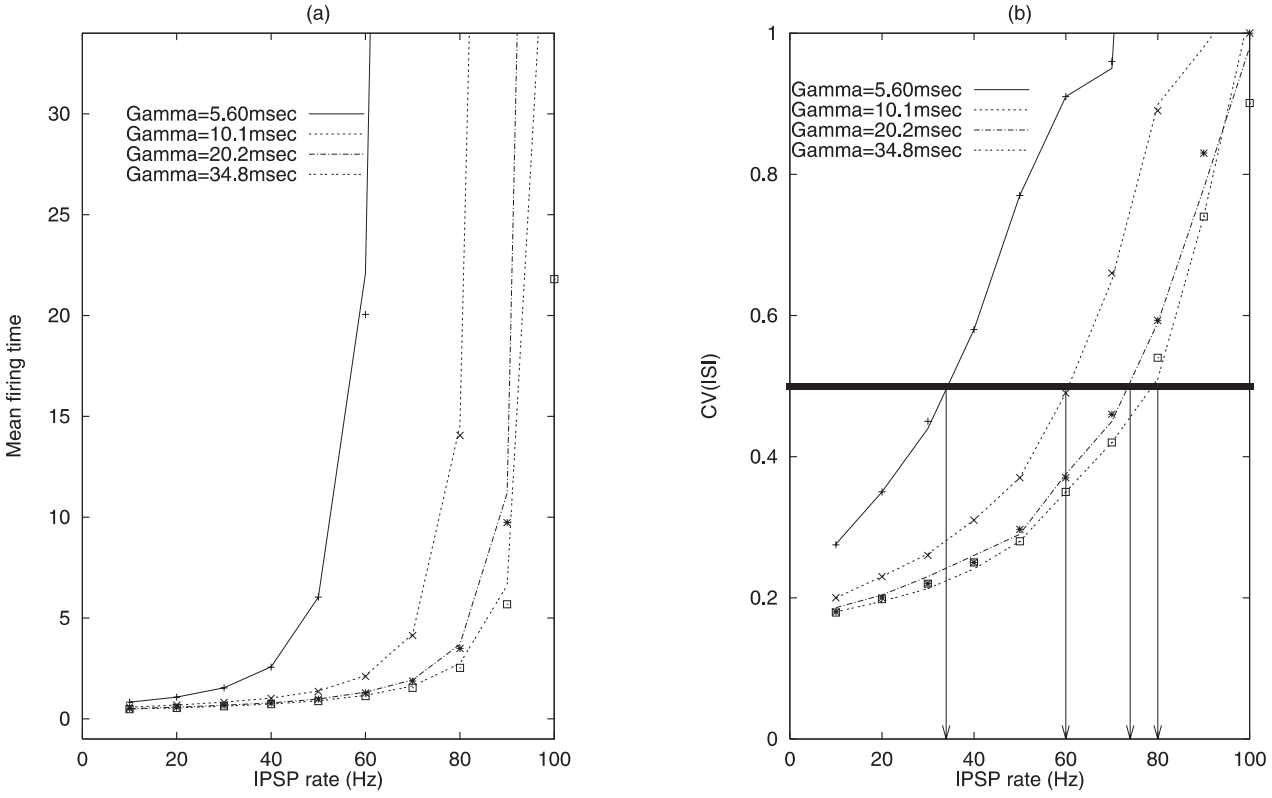

Fig. 1. Mean firing time and coefficient of variation (CV) for the two models V_t (*lines*) and v_t (*points*), $\lambda_E = 100$. We numerically simulate CV and firing time of v_t and V_t at $\lambda_I = 10, 20, \ldots, 100$ for $N_E = N_I = 100$. When the ratio $r = \lambda_I/\lambda_E$ is small both firing time and CV of V_t and v_t are close. λ_I^d is defined as the point at which CV equals 0.5 and indicated by *arrows*, from *left* to *right*, for comparison with Fig. 2

Stein's model with Poisson process inputs can be written in this formulation, with deterministic component $y_t = EV_t$ given by

$$dy_t = -\frac{1}{\gamma}(y_t - V_{\text{rest}})dt + \mu\, dt \tag{8}$$

and stochastic component ($\sigma = 1$)

$$d\bar{M}_t = a(dN_t^E - N_E\lambda_E\, dt) - b(dN_t^I - N_I\lambda_I\, dt) \tag{9}$$

When we say a state y is an attractor of the deterministic part of V_t we mean that y is an attractor of the dynamics (8).

3 Results: Stein's model

We first consider Stein's model and then move (in the next section) to a model with reversal potentials. For convenience of discussion, we have fixed a few parameters: $N_E = 100 = N_I$ (see [30] for a discussion of this choice), $\lambda_E = 100\,\text{Hz}$ [1], and γ lies within the range $20.2 \pm 14.6\,\text{ms}$ [22]. Hence the rate of total excitatory inputs is 10,000 Hz, which is approximately equivalent to 300×33 Hz due to the properties of the Poisson process, i.e. $N'_E = 300$ and $\lambda'_E = 33$. In [30] the authors employ $N'_E = 300$ in their simulations. Furthermore, in our simulations, γ takes the values 5.6, 10.1, 20.2, 34.8 ms. As pointed out in the previous section, it is hard to find an informative analytical formula for the first exit time of V_t from $(-\infty, V_{\text{th}}]$.

3.1 Predicting CV

A direct check on the dynamics defined by (1) shows that there are two essentially different cases:

1. $V_{\text{th}} > \mu\gamma + V_{\text{rest}}$, i.e. the threshold is above the position of the attractor y of the deterministic part given by
$$-(y - V_{\text{rest}})/\gamma + \mu = 0 \tag{10}$$
The process starting from V_{rest} will initially be driven by the deterministic force $-(y_t - V_{\text{rest}})/\gamma\, dt + \mu\, dt$ to approach $\mu\gamma + V_{\text{rest}}$, while also fluctuating with a random motion $d\bar{M}_t$ about this trajectory. Once, the membrane potential reaches $\mu\gamma + V_{\text{rest}}$, the deterministic force – tending either to depolarize or hyperpolarize the membrane potential – becomes zero. The random fluctuations cause the membrane potential to fluctuate around $\mu\gamma + V_{\text{rest}}$ and threshold crossings occur purely as a result of these random fluctuations. We then expect the efferent spike train to be irregular.
2. $V_{\text{th}} < \mu\gamma + V_{\text{rest}}$. In this case, the membrane potential would cross the threshold as a result of the deterministic force $-(y_t - V_{\text{rest}})/\gamma\, dt + \mu\, dt$ alone, but its trajectory is modified by random fluctuations. We expect then that the efferent spike trains would be quite regular.

Note that this analysis does not involve the well-known theory of random perturbations (see [3] for a complete description, [29, 35, 37]) where the random force becomes small, and the trajectories of the random processes concentrate around the deterministic trajectories. Then, only with a small probability does the random process deviate from the deterministic process. As a consequence its CV approaches zero. In the model we consider here, the variation of the random term is always greater than $a\sqrt{N_E\lambda_E}$. This large random force will always introduce appreciable and significant 'noise' into the model.

How does the nature of the synaptic inputs relate to whether $(V_{th} - V_{rest}) < \mu\gamma$ or $> \mu\gamma$? According to the definition of μ, we see that the threshold condition $(V_{th} - V_{rest}) = \mu\gamma$ is equivalent to $\lambda_E - \lambda_I = (V_{th} - V_{rest})/(a\gamma N_E)$. Let us denote $\lambda_I^a = \lambda_E - (V_{th} - V_{rest})/(a\gamma N_E)$ as the critical point, the critical level of inhibitory input, at which the dynamical attractor equals the threshold. Starting from $\lambda_I = 0$ (see Fig. 2), i.e. input with only excitatory synapses, we see that the position of attractor w is above the threshold. For $\gamma = 5.60$ ms, $\lambda_I^a = 29$ is the critical point(indicated by arrow in Fig. 2): for $\lambda_I < 29$ the attractor is situated above the threshold; and vice versa for $\lambda_I > 29$. $\lambda_I^a = 61, 80, 89$ are the critical points for $\gamma = 10.1$ ms, $\gamma = 20.2$ ms and $\gamma = 34.8$ ms, respectively (indicated by arrows in Fig. 2). In particular, when an exact balance between excitatory and inhibitory inputs is attained, the attractor y is situated at the resting potential, i.e. there is no deterministic input from synaptic input at all.

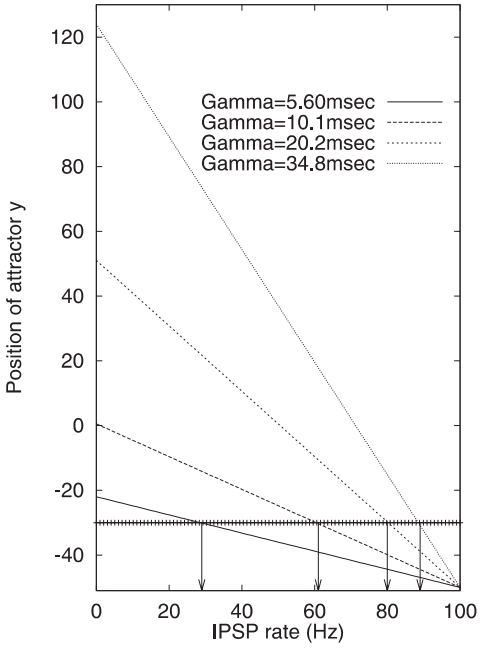

Fig. 2. Position of attractor y, a linear function of N_I, defined by (10) vs inhibitory postsynaptic potential (IPSP) rate, for $N_I = 100$ and total (EPSP) rate = 10,000 Hz. When there are only excitatory inputs, y is above the threshold (20 mV above resting potential which equals -30 mV) no matter what γ is, for sufficiently strong input intensity; a better balance between excitatory and inhibitory inputs pulls it down to the resting potential -30 mV. The values of λ_I^a at which the attractor is equal to the threshold are indicated by arrows for different $\gamma = 5.6, 10.1, 20.2$ and 34.8 ms (from *left* to *right*), by comparison with Fig. 1b

Table 1. λ_I^a and $[\lambda_I^d - 10, \lambda_I^d + 10]$ for $\gamma = 5.60, 10.1, 20.2, 34.8$ ms in Stein's model

γ (ms)	λ_I^a	$[\lambda_I^d - 10, \lambda_I^d + 10]$
5.60	29	[24, 44]
10.1	61	[50, 70]
20.2	80	[64, 84]
34.8	89	[70, 90]

3.2 Testing the predictions

Corresponding to the cases discriminated above, we carried out numerical simulations of Stein's model to determine whether the predictions about CV are correct. We find that the threshold (λ_I^a) at which CV is greater than 0.5 almost coincides with the threshold at which V_{th} becomes less than $V_{rest} + \mu\gamma$ as shown in numerical results (Fig. 1b).We summarise the numerical results in Table 1. More specifically, we have the following result:

$$\lambda_I^d - 10 < \lambda_I^a < \lambda_I^d + 10 \tag{11}$$

In conclusion, we see that CV is greater than 0.5 mainly due to random forces, the increase in which is caused by the increase in inhibitory synaptic inputs. When inhibitory inputs and excitatory inputs are poorly balanced, output CV is less than 0.5, whereas a good balance ensures a CV greater than 0.5. CV is thus a good indicator of the underlying dynamics: CV > 0.5 implies that the attractor is almost always below the threshold; CV < 0.5 that the attractor is almost always above the threshold. Finally, it is impossible to assert $\lambda_I^a = \lambda_I^d$ since when the attractor is close to the threshold, prediction of CV becomes uncertain because the 'noise' term $d\bar{M}_t$ is appreciable.

4 The model with reversal potentials

In this section we assume that $V_I = -60$ mV and $V_E = 50$ mV, values which match experimental data and, are used in the literature [23]. Again as in the literature [23], we impose a local balance condition on the magnitude of each excitating PSP (EPSP) and IPSP by $\bar{a}(V_E - V_{rest}) = \bar{b}(V_{rest} - V_I) = 1$ mV, i.e. starting from the resting potential, a single EPSP or a single IPSP will depolarize or hyperpolarize the membrane potential 1 mV above or below the resting potential. We also consider the case in which these expressions equal 0.5 mV.

4.1 Predicting CV in the presence of reversal potentials

The deterministic part of Z_t defined by (3) can be written as

$$dEZ_t = -\frac{EZ_t - V_{\text{rest}}}{\gamma}dt + [\bar{a}(V_{\text{E}} - EZ_t)N_{\text{E}}\lambda_{\text{E}} + \bar{b}(V_{\text{I}} - EZ_{\text{t}})N_{\text{I}}\lambda_{\text{I}}]dt \quad (12)$$

and the equilibrium state is given by

$$z = \frac{V_{\text{rest}}/\gamma + \bar{a}N_{\text{E}}\lambda_{\text{E}}V_{\text{E}} + \bar{b}N_{\text{I}}\lambda_{\text{I}}V_{\text{I}}}{1/\gamma + \bar{a}N_{\text{E}}\lambda_{\text{E}} + \bar{b}N_{\text{I}}\lambda_{\text{I}}} \quad (13)$$

As before we define λ_{I}^a as the value satisfying

$$V_{\text{th}} = \frac{V_{\text{rest}}/\gamma + \bar{a}N_{\text{E}}\lambda_{\text{E}}V_{\text{E}} + \bar{b}\lambda_{\text{I}}^a N_{\text{I}}V_{\text{I}}}{1/\gamma + \bar{a}N_{\text{E}}\lambda_{\text{E}} + \bar{b}\lambda_{\text{I}}^a N_{\text{I}}}$$

We have a similar situation (Fig. 3) as described above for Stein's model: a strong imbalance between excitatory and inhibitory inputs, i.e. an equivalent large deterministic input ensures the attractor z is above the threshold V_{th}; a better balance between excitatory and inhibitory inputs moves the attractor towards the resting potential, here -50 mV.

4.2 Testing the predictions

Numerical results are summarised in Table 2 for $V_{\text{th}} = -25$ mV (25 mV above the resting potential), $V_{\text{th}} = -30$ mV (20 mV above the resting potential) and $V_{\text{th}} = -35$ mV (15 mV above the resting potential). We see that a much better prediction than that of Stein's model (without reversal potentials) is obtained. For example, when $V_{\text{th}} = -30$ mV we have $\lambda_{\text{I}}^d \le \lambda_{\text{I}}^a \le \lambda_{\text{I}}^d + 2$. In other words in Stein's model with reversal potentials, λ_{I}^d is constrained to be closer to λ_{I}^a than in the same model without reversal potentials.

From numerical results (see Figs. 1b and 4), we see that one of the differences between Stein's model with and without reversal potentials lies in the former being much less sensitive to the decay rate $1/\gamma$ [19]. This could be understood from (4) and (2). If we rewrite (4) in the form

Table 2. λ_{I}^a and $[\lambda_{\text{I}}^d - 10, \lambda_{\text{I}}^d + 10]$ for $\gamma = 5.6, 10.1, 20.2$ and 34.8 ms, $V_{\text{th}} = -25$, -30 and -35 mV. Results for the case when $V_{\text{th}} = -30$ mV are plotted in detail in Figs. 3 and 4

γ (ms)	λ_{I}^a	$[\lambda_{\text{I}}^d - 10, \lambda_{\text{I}}^d + 10]$
5.60	9	[0, 20]
10.1	15	[5, 25]
20.2	18	[8, 28]
34.8	19	[9, 29]
	$V_{\text{th}} = -25$ mV	
5.60	15	[5, 25]
10.1	20	[11, 31]
20.2	23	[12, 32]
34.8	25	[13, 33]
	$V_{\text{th}} = -30$ mV	
5.60	23	[12, 32]
10.1	28	[14, 34]
20.2	31	[14, 34]
34.8	32	[16, 36]
	$V_{\text{th}} = -35$ mV	

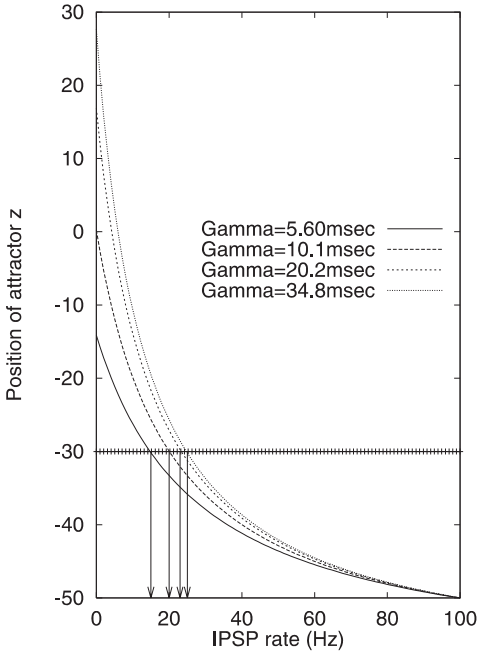

Fig. 3. Position of attractor z defined by (13) vs IPSP rate λ_{I}, $\lambda_{\text{E}} = 100$ with $\bar{a}(V_{\text{E}} - V_{\text{rest}}) = \bar{b}(V_{\text{rest}} - V_{\text{I}}) = 1$ mV, and $N_{\text{E}} = 100 = N_{\text{I}}$. When there are only excitatory inputs, z is above the threshold (-30 mV); a better balance between excitatory and inhibitory inputs moves it towards the resting potential -50 mV. λ_{I}^a – at which the position of attractor is equal to the threshold – is indicated by *arrows* for $\gamma = 5.6, 10.1, 20.2$ and 34.8 ms (from *left* to *right*)

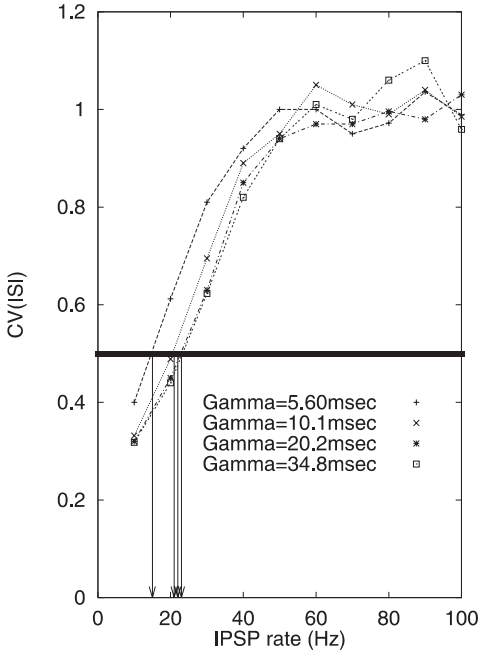

Fig. 4. CV in simulations of the reversal potentials model for the case $\bar{a}(V_{\text{E}} - V_{\text{rest}}) = \bar{b}(V_{\text{rest}} - V_{\text{I}}) = 1$ mV, $N_{\text{E}} = 100 = N_{\text{I}}$, $V_{\text{th}} = -30$ mV, calculated at $\lambda_{\text{I}} = 10, 20, \cdots, 100$ for $\gamma = 5.60$, $10.1, 20.2$ and 34.8 ms, and $\lambda_{\text{E}} = 100$. λ_{I}^d is defined as the point at which CV equals 0.5, indicated by *arrows*, for comparison with Fig. 3

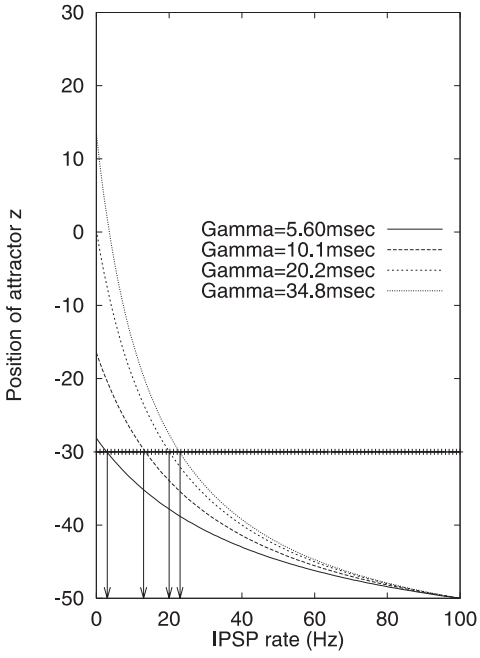

Fig 5. Position of attractor z defined by (13) vs IPSP rate λ_{I}, $N_{\mathrm{E}} = 100 = N_{\mathrm{I}}$, $\lambda_{\mathrm{E}} = 100$ Hz and $\bar{a}(V_{\mathrm{E}} - V_{\mathrm{rest}}) = a = 0.5\,\mathrm{mV} = \bar{b}(V_{\mathrm{rest}} - V_{\mathrm{I}}) = b$. λ_{I} at which the position of attractor is the same as the threshold is indicated by *arrows* for $\gamma = 5.6, 10.1, 20.2$ and 34.8 ms (from *left* to *right*)

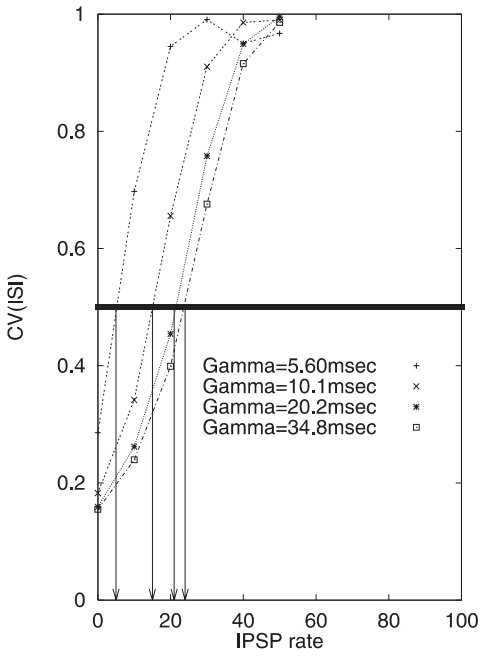

Fig. 6. CV vs IPSP rate λ_{I}, $\lambda_{\mathrm{E}} = 100$ Hz, and $\bar{a}(V_{\mathrm{E}} - V_{\mathrm{rest}}) = a = 0.5\,\mathrm{mV} = \bar{b}(V_{\mathrm{rest}} - V_{\mathrm{I}}) = b$. λ_{I} at which CV equals 0.5 is indicated by *arrows* for different $\gamma = 5.6, 10.1, 20.2$ and 34.8 ms (from *left* to *right*), for comparison with Fig. 5

$$
\begin{aligned}
dZ_t = & -\frac{Z_t - V_{\mathrm{rest}}}{\gamma}\,dt - \bar{a}(Z_t - V_{\mathrm{rest}})dN_t^{\mathrm{E}} - \bar{b}(Z_t - V_{\mathrm{rest}})dN_t^{\mathrm{I}} \\
& + \bar{a}(V_{\mathrm{E}} - V_{\mathrm{rest}})dN_t^{\mathrm{E}} + \bar{b}(V_{\mathrm{I}} - V_{\mathrm{rest}})dN_t^{\mathrm{I}} \\
= & -(Z_t - V_{\mathrm{rest}})\left(\tfrac{1}{\gamma}dt + \bar{a}\,dN_t^{\mathrm{E}} + \bar{b}\,dN_t^{\mathrm{I}}\right) \\
& + \bar{a}(V_{\mathrm{E}} - V_{\mathrm{rest}})dN_t^{\mathrm{E}} + \bar{b}(V_{\mathrm{I}} - V_{\mathrm{rest}})dN_t^{\mathrm{I}} \qquad (14)
\end{aligned}
$$

we see that in the model with reversal potentials, there are three 'leakage' terms: the first is $(Z_t - V_{\mathrm{rest}})/\gamma\,dt$, the second and the third are $\bar{a}(Z_t - V_{\mathrm{rest}})dN_t^{\mathrm{E}}$ and $\bar{b}(Z_t - V_{\mathrm{rest}})dN_t^{\mathrm{I}}$, respectively. The latter two terms are stronger than the first term (see the range of γ at the end of Sect. 2), i.e. the model with reversal potentials tends to forget much faster than Stein's model without reversal potentials and, at the same time, to ensure its activity is less sensitive to the decay rate. Another advantage of (14) is that we can apply the comparison theorem in stochastic differential equations. We expect that application of this theorem would provide a theoretical answer to a current debate about whether the tail of the output interspike interval distribution is long or short [37, 34].

The EPSP and IPSP sizes used in the simulations above for the model with reversal potentials are 1 mV when $Z_t = V_{\mathrm{rest}}$. However, we use 0.5 mV for the model without reversal potentials. Of course, they are not completely comparable since for the model with reversal potentials, the term $\bar{a}(V_{\mathrm{E}} - V_t)$ $(\bar{b}(V_t - V_{\mathrm{I}}))$ change when V_t moves away from V_{rest}. In particular, when $V_t = V_{\mathrm{I}}$, then the term $\bar{b}(V_t - V_{\mathrm{I}})$ vanishes. However, we also consider the case when $\bar{a}(V_{\mathrm{E}} - V_{\mathrm{rest}}) = a = \bar{b}(V_{\mathrm{rest}} - V_{\mathrm{I}}) = b = 0.5$ mV. In Figs. 5 and 6 we show numerical simulations for this case. It is readily seen that λ_{I} at which the position of attractor is the same as the threshold coincides well with the value at which CV equals 0.5.

5 Discussion

Inputs in the present paper are exclusively Poisson process [8], which indicates that all conclusions above are true if we fix input rates $\lambda_{\mathrm{E}} = 100$ Hz, $\lambda_{\mathrm{I}} = 100$ Hz and $N_{\mathrm{E}} = 100$ and replace λ_{I} by N_{I} as a parameter. In recent years there has been much research devoted to answering the following question (see [8] and references therein): whether there is a region of N_{I}, in agreement with anatomical data, in which the model generates CV greater than 0.5. We note here that in the model with reversal potentials, CV is greater than 0.5 for most values of N_{I}, and similar phenomena have been observed in the literature [18, 23, 33]. For example, when $\gamma = 20.2$ ms and $V_{\mathrm{th}} = -30$ mV, as soon as $N_{\mathrm{I}} > N_{\mathrm{I}}^d = 25$, i.e. $N_{\mathrm{I}}/N_{\mathrm{E}} > 0.25$, CV is greater than 0.5. In our analysis we have considered the case $\lambda_{\mathrm{I}} = \lambda_{\mathrm{E}}$. A more efficient IPSP input will reduce N_{I}^d further, remembering that the typical composition of cortical tissue is about $N_{\mathrm{I}}/N_{\mathrm{E}} = 1/6 \sim 0.17$ [1]. Therefore, in terms of simple statistical quantities like CV, there is no contradiction between the output of theoretical models and experimental data [28]. Furthermore, to produce a CV greater than 0.5, it is not necessary to go to the extreme case: an exact balance between excitatory and inhibitory inputs as discussed in [30, 36] is not needed.

Many analytical, numerical and simulation studies have attempted to predict how CV of efferent spike trains greater than 0.5 might arise for the integrate-and-fire model [11, 18, 19, 28, 30, 32, 33, 35]. Some of these studies are particularly concerned with the accuracy and utility of diffusion approximations (see Sect. 2.3). None, so far as we are aware, relate CV to the position of the attractor of the deterministic part of the dynamics as we have done here. In this paper based upon the simplest model of a single neurone (Stein's model) and the equivalent model with reversal potentials, we find that when the position of the attractor of the deterministic part is below the threshold, CV is greater than 0.5; and vice versa when the attractor is above the threshold. In other words, in the former case, neuronal firing is then due to purely stochastic forces. There has been much research concerned with the role of noise in neurodynamics [3–5, 10, 16]. Here for the first time, by analysing the mechanisms of neuronal activity in a very simple canonical model, we clarify another role played by stochastic forces. A separate question of course is why neurones employ stochastic forces rather than the more reliable deterministic forces to cross the threshold and hence to process information. The question may only be clearly answered when we more fully understand the brain.

Acknowledgements. We are grateful to Martin Baxter and an anonymous referee for their valuable comments. The work reported in this paper was financially supported by the BBSRC and the Royal Society.

References

1. Abbott LF, Varela JA, Sen K, Nelson SB (1997) Synaptic depression and cortical gain control. Science 275:220–223
2. Abeles M (1990) Corticonics. Cambridge University Press, Cambridge, UK
3. Albeverio S, Feng J, Qian M (1995) Role of noises in neural networks. Phys Rev E 52:6593–6606
4. Arieli A, Sterkin A, Grinvald A, Aertsen AD (1996) Dynamics of ongoing activity: explanation of the large variability in evoked cortical responses Science 273:1868–1871
5. Bezrukov SM, Vodyanoy I (1997) Stochastic resonance in non-dynamical systems without response thresholds. Nature 385:319–321
6. Feng J (1996) The hydrodynamic limit for the reaction diffusion equation – an approach in terms of the GPV method. J Theor Probab 9:285–299
7. Feng J (1997) Behaviours of spike output jitter in the integrate-and-fire model. Phys Rev Lett 79:4505–4508
8. Feng J, Brown D (1998) Impact of temporal variation and the balance between excitation and inhibition on the output of the perfect integrate-and-fire model. Biol Cybern 78:369–376
9. Feng J, Lei G, Qian M (1992) Second-order algorithms for SDE. J Comput Math 10:376–387
10. Ferster D (1996) Is neural noise just a nuisance? Science 273:1812
11. Hanson FB, Tuckwell HC (1983) Diffusion approximation for neuronal activity including synaptic reversal potentials. J Theor Neurobiol 2:127–153
12. Hertz J (1999) Reading the information in the outcome of neural computation. In Building blocks for intelligent systems (in press)
13. Holden AV (1976) Models of the stochastic activity of neurones. Springer, Berlin, Heidelberg, New York
14. Holt GR, Softky WR, Koch C, Douglas RJ (1996) Comparison of discharge variability in vitro and in Vivo in cat visual cortex neurons. J Neurophysiol 75:1806–1814
15. Hopfield JJ, Herz AVM (1995) Rapid local synchronization of action potentials: towards computation with coupled integrate-and-fire networks. Proc Natl Acad Sci USA 92:6655–6662
16. Jung P, Wiesenfeld K (1997) Too quite to hear a whisper Nature 385:291
17. Koch C (1997) Computation and the single neurone Nature 385:207–210
18. Lánský P, Musila M (1991) Variable initial depolarization in Stein's neuronal model with synaptic reversal potentials. Biol Cybern 64:285–291
19. Lánský P, Sacerdote L, Tomassetti F (1995) On the comparison of Feller and Ornstein-Uhlenbeck models for neural activity. Biol Cybern 73:457–465
20. Mainen ZF, Sejnowski TJ (1995) Reliability of spike timing in neocortical neurones. Science 268:1503–1506
21. Mainen ZF, Sejnowski TJ (1996) Influence of dendritic structure on firing pattern in model neocortical neurones. Nature 382:363–366
22. McCormick DA, Connors BW, Lighthall JW, Prince DA (1985) Cooperative electrophysiology of pyramidal and sparsely spiny stellate neurons of the neocortex. J Neurophysiol 54:782–805
23. Musila M, Lánský P (1994) On the interspike intervals calculated from diffusion approximations for Stein's neuronal model with reversal potentials. J Theor Biol 171:225–232
24. Ricciardi LM, Sato S (1990) Diffusion process and first-passage-times problems. Lectures in applied mathematics and informatics. Manchester University Press, Manchester
25. Rieke F, Warland D, Ruyter van Steveninck R, de Bialek W (1997) Spikes – exploring the neural code. MIT Press, Cambridge, Mass
26. Ruyter van Steveninck RR de, Lewen GD, Strong SP, Koberle R, Bialek W (1997) Reproducibility and variability in neural spike trains. Science 275:1805–1808
27. Sejnowski TJ (1995) Time for a new neural code? Nature 323:21–22
28. Softky W, Koch C (1993) The highly irregular firing of cortical-cells is inconsistent with temporal integration of random EPSPs. J Neurosci 13:334–350
29. Smith CE (1992) A heuristic approach to stochastic models of single neurons. In: McKenna T, David J, Zorrnetzer SF (eds) Single neuron computation. Academic Press, San Diego, 561–588
30. Shadlen MN, Newsome WT (1994) Noise, neural codes and cortical organization Curr Opin Neurobiol 4:569–579
31. Thomson AM (1997) Activity-dependent properties of synaptic transmission at two classes of connections made by rat neocortical pyramidal. J Physiol 502:131–147
32. Troyer TW, and Miller KD (1997) Physiological gain leads to high ISI variability in a simple model of a cortical regular spiking cell. Neural Comput 9:733–745
33. Tuckwell HC (1979) Synaptic transmission in a model for stochastic neural activity. J Theor Biol 77:65–81
34. Tuckwell HC (1988) Stochastic processes in the neurosciences. Society for Industrial and Applied Mathematics, Philadelphia
35. Tuckwell HC, Richter W (1978) Neuronal interspike time distributions and the estimation of neurophysiological and neuroanatomical parameters. J Theor Biol 71:167–183
36. Vreeswijk C van, Sompolinsky H (1996) Chaos in neuronal networks with balanced excitatory and inhibitory activity. Science 274:1724–1726
37. Wan FYM, Tuckwell HC (1982) Neuronal firing and inputs variability. J Theor neurobiol 1:197–218
38. Wilbur WJ, Rinzel J (1983) A theoretical basis of large coefficient of variation and bimodality in neuronal interspike interval distribution. J Theor Biol 105:345–368